COBEM 2023 27TH INTERNATIONAL CONGRESS OF MECHANICAL ENGENEERING

ABCM Brazilian Society of Mechanical Sciences and Engineering
27th ABCM International Congress of Mechanical Engineering
December 04-08, 2023, Florianópolis-SC, Brazil

COB-2023-0222
NUMERICAL VERIFICATION OF A PARALLELIZED CODE RUN ON GPU APPLIED TO MOVING HEAT SOURCE AUTOGENOUS WELDING PROCESSES

Ernandes José Gonçalves do Nascimento
Arthur Mendonça de Azevedo
Elisan dos Santos Magalhães
Instituto Tecnológico de Aeronáutica – ITA, 12228-900, São José dos Campos – SP, Brasil
ernandes@ita.br
arthurama@ita.br
elisan@ita.br

Luiz Eduardo dos Santos Paes
Federal University of Uberlândia – UFU, 38410-337, Uberlândia – MG, Brasil
luiz.paes@ufu.br

Abstract. *The industrial revolution fostered by the application of the Computational Fluid Dynamics (CFD) techniques had made possible a series of enhancements in modern engineering design. The recent advancements in processing hardware gave room for the modeling and simulation of a variety of higher complexity physical phenomena. However, although there has been a recent significative increase in hardware parallel computing performance, most CFD codes still make use of very limited serial-based processing methodologies. The arithmetic operations accuracy and the execution advantages of developing a numerical solution through parallel Graphics Processing Unit (GPU) computing has been put in question for years in the scientific community. To fulfill this gap, a numerical verification of an inhouse parallelized (Compute Unified Device Architecture) CUDA-C language code was performed. A moving heat source autogenous welding process was simulated to compare the GPU processed data to a commercial code solution. The analysis here was performed by applying the Finite Volume Method (FVM) to solve the transient heat conduction Partial Differential Equation (PDE) in a fixed structured uniform mesh. A first order temporal discretization scheme and temperature dependent thermal properties were applied in the solutions. The melting and solidification processes were accounted for by the application of the enthalpy method. The moving heat source was modeled through a time and space dependent Gaussian whole conical volumetric heat distribution profile. A Nvidia Geforce® RTX™ 3090 graphics card with 24 GB of dedicated memory was applied as the inhouse code processing hardware. The commercial code solutions were run on an Intel® Core™ I7 11700K with a 3.6 GHz base clock and 16 parallel processing threads. The research outcomings suggested that GPU processing deliveries a similar computational accuracy to that of a CPU but a much higher efficiency in hardware usage. The results also evidenced that CPU parallelization does have an optimum number of simultaneously run processes that is far below its hardware maximum number of threads.*

Keywords: *GPU processing, CUDA-C language, Finite Volume Method, Autogenous welding, Numerical phase change.*

1. INTRODUCTION

Numerical methods have revolutionized modern research and development by enabling scientists and engineers to solve complex mathematical models digitally. The advancements achieved through innovative Computational Fluid Dynamics (CFD) algorithms during the last decades had made possible the simulation of real-world phenomena with higher accuracy and processing efficiency. By applying the conservation of mass, momentum, energy, and species mass at a discrete physical domain one may predict fluid flow, heat and mass transfer, chemical reactions and related multiphysics, which is not always possible using other methodologies. For instance, Aboul Khail and Erisen (Aboul Khail & Erien, 2023) had recently dissertated about the difficulties in analyzing and studying the heat transfer in Plate Heat Exchangers (PHEs) analytically due to its complex geometry type. Hence, this matter is usually addressed by numerical methods, which have proven to be reliable in solving different flow types at different conditions and geometries. Adding to the previous considerations, Ju et al. (Ju, Li, & Wang, 2022) pointed out that CFD has also become the main method for prediction of the properties of the external wind environment in cities and other urban contexts. In this case, CFD offers the great advantage of building actual scale simulation models, compared to the traditional reduced scale wind tunnel models often applied in studies in the field (Montazeri & Blocken, 2013). The two past examples may be found among many similar occurrences that illustrate the versatility and the growth in CFD popularity in the last three decades.

Following the evolutionary timeline of the numerical methods, the recognition of the field as a mathematical discipline only happened in the 20th century. The book written by Professor Whittaker and Robinson (Whittaker & Robinson, 1924) is often credit by many as the origin of modern numerical analysis. The content produced by the authors is aligned with attempts to find approximate solutions of problems instead of exact ones. Nonetheless, it is important to recap that the invention of Digital Electronic Computers (DEC) dates from mid 1940s, with hand, slide ruler, desk calculators and mechanical calculators being the applied tools at previous times. The advent of DEC and the participation of large numbers of mathematicians in the second world war effort gave room to the first computations of previously developed numerical approaches, such the Finite Difference Methods (FDM) for representing solutions of Partial Differential Equations (PDEs). Hence, the development of the modern FDM technique may be considered an evolution of the works performed by Richardson (Richardson, 1910), Phillips and Wiener (Philips & Wiener, 1923) and Courant et al. (Courant, Friedrichs, & Lewy, 1928). The work by Courant et al. demonstrated the use of FDM not to solve practical problems but to instead stablish existence uniqueness of results for elliptic boundary value and eigenvalue problems, and for the initial value problem for hyperbolic and parabolic PDEs. The work also introduced the method of random walks for approximating the solution of PDEs and ended up influencing the development of Monte Carlo methods for evaluating the same type of differential equations (Curtiss, 1953). Courant was also responsible for another influential paper published during the second world war, (Courant, Variational Methods for the Solution of Problems of Equilibrium and Vibrations, 1943). According to Benzi (Benzi, 2009), the ideas presented in just 1943 represent a few of the main aspects contained in the Finite Element Methods (FEM). However, the full development of FEM only happened during the 1960s, with the participation of the aerospace and civil engineers Clough and Felippa (Clough & Felippa, 1968), Cheung and Zinkiewicz (Cheung & Zinkiewicz, 1965) and Irons and Barlow (Irons & Barlow, 1964).

Although the FDM is a discretization scheme still widely applied in modern CFD it offers the main disadvantage of not conserving the mass and energy fluxes transferred between neighbor cells. Due to a new approach proposed to bypass this problem, Patankar (Patankar, 1980) ended up placing himself among the most important CFD pioneers. The author became widely known for the development of the Finite Volume Method (FVM), which has the main advantage of being an energy and mass conservative discretization scheme. The Semi-Implicit Method for Pressure-Linked Equations (SIMPLE) is credited by many to be the most important contribution of the author's career. This algorithm is still one of the main applied numerical procedures to solve the Navier-Stokes equations. Patankar still contributed more by publishing in 1979 a modified variant of the algorithm known as the SIMPLER (SIMPLE Revised).

The pioneer achievements previously cited have indeed revolutionized the development of numerical methods. However, the solution processing of such techniques is highly dependent on hardware optimization, which still leaves to the present day plenty of room for new parallelized computational methods. Specifically in respect to welding processes simulation, Ikushima and Shibahara (Ikushima & Shibahara, 2014) proposed the Idealized Explicit Finite Element Method (IEFEM) for shorter computing time and lower memory consumption analyzed through a simple T-joint problem. In addition, the authors had also implemented code parallelization run using a GPU. The results yielded that the final computing time and memory consumption were 1/250 and 1/130, respectively, that of that of a static implicit FEM for a problem with 96,500 nodes. Ma (Ma, 2016) developed a GPU parallelized code to simulate the thermal stress and welding deformation in large structure models. The author employed the FEM with a two-stage computation scheme where the first approach was based on a dynamic explicit method applied by controlling both the temperature increment and the time scaling parameter. For the second scheme, a static equilibrium computation method was implemented. The GPU solution developed demonstrated to have good scalability and accuracy for large scale models of more than 20 million degrees of freedom. In previous work, de Azevedo et al. (de Azevedo, Magalhães, da Silva, & Lima e Silva, 2022) performed a comparison between nonlinear and constant thermal properties approaches to estimate the temperature in Laser Beam Welding (LBW) simulation. The authors presented a detailed study of the temperature gradient, its influence on thermocouples positioning, and a methodology for the thermal properties convergency evaluation. The results presented were however not intensively compared in terms of performance and accuracy to well stablished commercial code solutions. Zhang et al. (Zhang, et al., 2023) has recently developed hybrid Message Passing Interface (MPI) and CUDA paralleled unstructured CFD simulations on a multi-GPU system. The authors applied the FVM to solve an explicitly discretized compressible flow problem. Some strategies were applied for optimizing indirect data access, with both packing and unpacking data for communication being performed on the GPU. The research results yielded an increase in kernels' performance of 40 – 60% due to cell and face renumbering optimization on the global data location.

As observed in the past literature review, very consistent advancements were made since the beginning of development of the numerical methods. However, there is clearly an evolutionary discrepancy between the updates in hardware and commercially available CFD codes. The CPU-based processing methodologies have been researched and developed for more than fifty years, whereas GPU processing has barely reached ten years on real development. Even so, most GPU based published works are rarely focused on welding modeling and scarcely ever embrace FVM through implicit temporal discretization schemes. Additionally, very few published simulations present intensive accuracy and performance comparisons to top rated commercial codes. Hence, the present research was aimed at developing a deep verification process of a parallelized GPU code. Here, the high industrial value problem of automated LBW was simulated to exemplify the effectiveness of the implemented methodology. The heat source was modeled as a moving Gaussian whole conical profile. The main simulations were performed in an inhouse CUDA-C language code and run in a Nvidia™

Geforce® RTX™ 3090 with 24 GB of video memory. A Geforce® RTX™ 4090 with 24 GB of video memory was also used in the performance study to enrich the analysis. The heat conduction Partial Differential Equation (PDE) with a transient total enthalpy term was spatially discretized in a three-dimensional domain and converted into an algebraic equation by the application of the FVM. The melting process was accounted for through the enthalpy method. Variations of constant and temperature dependent thermal properties were applied to the welded specimens' material. The Successive over-relaxation (SOR) parallelized solver was used to solve the coefficients matrix equation. The thermal modeling accounted for radiation and convection losses during the welding process. Three equivalent solutions produced by commercially well succeeded CPU based codes were run on an Intel® Core™I7 11700K 3.6 GHz processor and included in the final discussion to compare the processing performance and accuracy of the simulated results. The research outcomings evidenced the great performance of GPUs for CFD purposes and suggested that the exposed methodology has plenty of potential to replace traditional serial-based methods.

2. MATERIALS AND METHODS

2.1 The Laser Beam Welding (LBW) Problem

Modern LBW is currently one of the most important manufacturing processes. The union of materials by using a concentrated light beam as heat source is also the most simulated welding process, as statistically analyzed in previous work (Nascimento, Magalhães, & dos Santos Paes, 2023). The recent growth in its use among similar industrial methods has contributed to subside further developments of such technique. Here, the process was simulated by modeling an automated laser head focused on a SAE 1020 specimen. The LBW process simulated and its important geometrical parameters and thermophysical considerations are schematized in Figure 1, where L_x, L_y and L_z are the specimen length at x, y and z directions, respectively, L_w is the weld bead length, u is the laser head velocity, T_∞ is the ambient temperature, Q_{rad} is the rate of heat loss by radiation and Q_{con} is the rate of heat loss by convection.

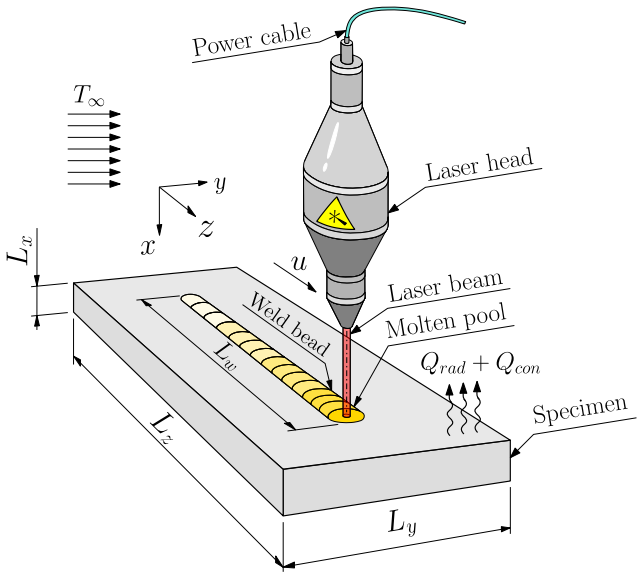

Figure 1. Laser Beam Welding (LBW) process schematics and thermophysical modeling.

The welding process parameters depicted in Figure 1 are tabulated in Table 1.

Table 1. Welding process parameters.

Parameter	Values
Specimen length at x, y and z-directions (L_x), (L_y) and (L_z) [mm]	9.5, 20.0 and 40.0
Weld bead length (L_w) [mm]	30.0
Laser head velocity (u) [mm/min]	3000.0
Ambient Temperature (T_∞) [ºC]	20.0

2.2 Heat Transfer Model

The investigated problem physics are mainly governed by the three-dimensional transient heat conduction equation. Here, the expression is set as a PDE with a volumetric heat rate generation term and the transient term written as a function of the total enthalpy. Hence, the model may be cast as

$$\frac{\partial}{\partial x}\left(\lambda\frac{\partial T}{\partial x}\right)+\frac{\partial}{\partial y}\left(\lambda\frac{\partial T}{\partial y}\right)+\frac{\partial}{\partial z}\left(\lambda\frac{\partial T}{\partial z}\right)+\dot{g}=\frac{\partial H}{\partial t} \tag{1}$$

where x, y and z are the cartesian coordinates, T is the numerical temperature, λ is the non-linear thermal conductivity, $\dot{g}$ is the volumetric heat source and t is the time. The quantity H is the total enthalpy, which can be written as (Crank, 1984),

$$H=\underbrace{\rho\int_0^T c_p\left(\phi\right)d\phi}_{\substack{\text{portion related to}\\ \text{the sensible heat}}}+\underbrace{\rho f_L\left(T\right)L_f}_{\substack{\text{portion related to}\\ \text{the latent heat}}} \tag{2}$$

where ρ is the density, c_p is the specific heat at constant pressure, f_L is the temperature dependent liquid mass fraction function, ϕ is the generic integration variable and L_f is the latent heat of fusion. The Heaviside step function, f(T), was applied to calculate the material fusion. This equation may be written as

$$f_L\left(T\right)=\begin{cases}1 \text{ if } T>T_m\\ 0 \text{ if } T<T_m\end{cases} \tag{3}$$

where T_m is the melting temperature. The heat losses by convection and radiation were calculated based on the Newton's law of cooling and the Stephan Boltzmann law, respectively. The final heat loss equation may be written as

$$\frac{\partial T}{\partial \eta}=\underbrace{h(T)\left(T-T_\infty\right)}_{\substack{\text{Newton's law}\\ \text{of cooling}}}+\underbrace{\sigma\phi_{rad}(T)\left(T^4-T_\infty^4\right)}_{\text{Stephan Boltzmann law}} \tag{4}$$

where η is the direction normal to the surface, $h(T)$ is the temperature dependent heat transfer coefficient, σ is the Stefan Boltzmann constant and ϕ_{rad} the material's emissivity.

2.3 Automated Heat Source

The moving heat source was modeled as a Gaussian whole conical volumetric profile, as defined, and reviewed in previous work (Nascimento, Magalhães, & dos Santos Paes, 2023; Magalhães, et al., 2018). The mathematical modeling of the heat distribution may be written as

$$\dot{g}=\frac{Q_W}{0.460251h_pR^2}e^{-\frac{4.5\left(z-ut\right)^2}{R^2}}e^{-\frac{4.5\left(y-L_y/2\right)^2}{R^2}}\left(1-\frac{x^{1/2}}{h_p^{1/2}}\right) \tag{5}$$

where Q_w is the laser heat source power, h_p is the height of penetration, R is the welding radius and u is the laser head velocity (Table 1). The final heat source model and its parameters are schematized in Figure 2.

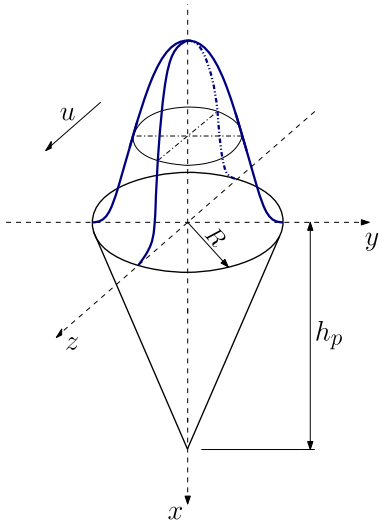

Figure 2. Gaussian whole conical volumetric heat source.

The heat source model parameters presented in Figure 2 are tabulated in Table 2.

Table 2. Heat source model parameters.

Parameter	Values
Welding radius (R) [mm]	0.5
Height of penetration (h_p) [mm]	1.65
Laser power (Q_w) [W]	400.0, 1200.0

2.4 Simulation Parameters, Mesh and Data Probe

The applied temporal parameters in the simulation are tabulated in Table 3.

Table 3. Simulation temporal parameters.

Parameter	Values
Temporal discretization	First order scheme
Time-step (Δt) [s]	1.0×10^{-3} and 2.5×10^{-5}
Simulation total time (t_{Tot}) [s]	2.5

The physical domain was built as a uniform orthogonal structured mesh. A grid size independence study was addressed to assure results independent of spatial refinement. The simulation outputs became independent of the grid at nearly 3,000,000 total nodes, in proportion to the specimen lengths at each dimension. Hence, a final mesh with 3,203,904 total nodes was instead used (82 × 148 × 264 nodes, at x, y and z, respectively), resulting in an added safety factor of approximately 6.797 %. A time-step size independence analysis with fixed values was also addressed. Results became independent of temporal grid refinement for values smaller than 5×10^{-3} s. However, the values of 1×10^{-3} and 2.5×10^{-5} s were instead applied to the set of results in subsections 3.1 and 3.2, respectively, in direct proportion to the applied heat source power [W]. Larger time-step values in both analyses will indeed result in either significative inaccuracies or solver failure.

The probe points $\boldsymbol{P_1}$ to $\boldsymbol{P_4}$ were positioned transversally to the weld bead to measure the resultant temperature fields and compare the outcomings processed by each code. The cartesian coordinates for each of the four probe points are presented in Table 4.

Table 4. Probe points cartesian coordinates.

Coordinates	P_1	P_2	P_3	P_4
x [mm]	9.5	9.5	9.5	9.5
y [mm]	10.0	11.0	12.0	13.0
z [mm]	20.0	20.0	20.0	20.0

2.5 Material Properties

The LBW process was performed on a SAE 1020 specimen. Variations of constant and temperature dependent properties were applied during the code verification process for the thermal conductivity (λ) and the specific heat (c_p).

The corresponding values of the temperature dependent properties at 20 °C were used whenever constant properties were applied. The thermophysical properties of the welded material are presented in Table 5.

Table 5. SAE 1020 steel thermophysical properties.

Thermal properties (SAE 1020)	**Values / Equations**
Density (ρ) [kg/m³]	7,731.3
Thermal conductivity (λ) [W/m.K]	$\lambda(T) = 2.5\times10^{-5}T^2 - 0.053T + 57.2$
Specific heat (c_p) [J/kg.K]	$c_p(T) = 3.298\times10^2 e^{1.509\times10^{-3}T}$
Emissivity (ϕ_{rad})	0.8
Latent heat of fusion (L) [kJ/kg]	247.0
Melting Temperature (T_m) [°C]	1450.0

The temperature dependent behavior of the SAE 1020 thermal properties is illustrated in Figure 3.

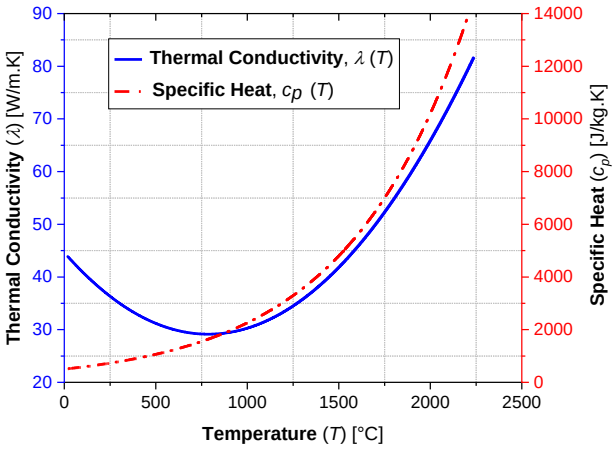

Figure 3. Temperature dependent thermal properties behavior.

3. RESULTS AND DISCUSSION

3.1 Heat Conduction

The first set of results was produced aiming the verification of the heat conduction results accuracy of each code. Hence, the heat source laser power (Q_w) was reduced to only 400.0 [W] to avoid reaching the melting temperature (T_m) of the specimen. Firstly, the investigation was performed by applying constant thermal properties to facilitate curves matching and consequently assure a completely equal set of material properties, variables, and any other parameters in all codes. The plots presented in Figure 4 depicts the overall great convergence achieved between the probed temperatures at the points P_1 and P_4 for all solutions ran. The average absolute error (E_{avg}) [%] between the CUDA® code and each commercial solution was also calculated, and its values are included in Table 6. The maximum average absolute error reached was 2.613 % between CUDA® code and commercial code #2, for probe point P_1.

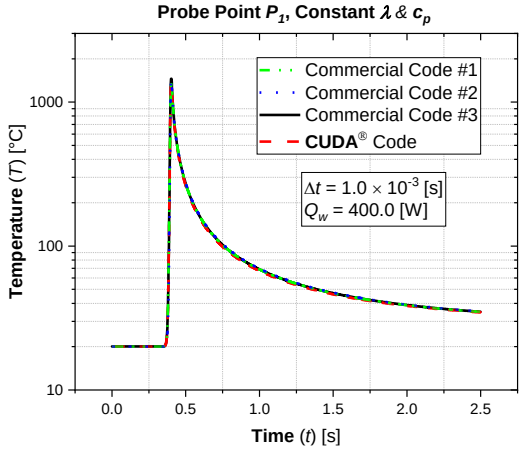

a)

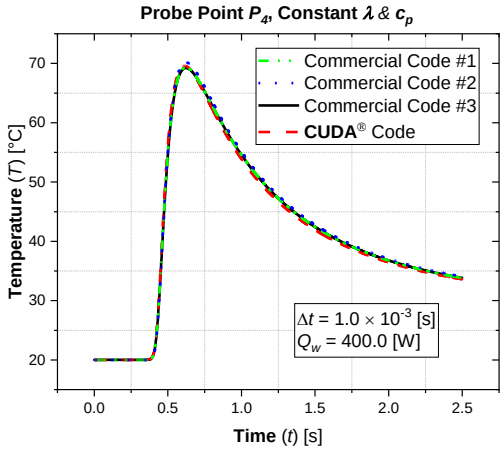

b)

Figure 4. Temperature (T) [°C] as a function of time (t) [s] for 400 [W] laser power (Q_w), 1.0 × 10^{-3} [s] time-step size (Δt), constant λ and c_p and: a) Probe point $\boldsymbol{P_1}$, b) Probe point $\boldsymbol{P_4}$.

Table 6. Average absolute error (E_{avg}) [%] between CUDA® code and each commercial solution.

Solution	P_1 - Average Error (E_{avg}) [%]	P_4 - Average Error (E_{avg}) [%]
Commercial Code #1	1.634	0.914
Commercial Code #2	**2.613**	1.616
Commercial Code #3	1.674	0.940

Continuing with the investigation, the simulations were run again with constant specific heat (c_p) and temperature dependent thermal conductivity (λ). The temperature convergence between all solutions is illustrated in Figure 5. The maximum average error reached was 12.572 % between CUDA® code and commercial code #3 for probe point P_2. The average error values are tabulated in Table 7.

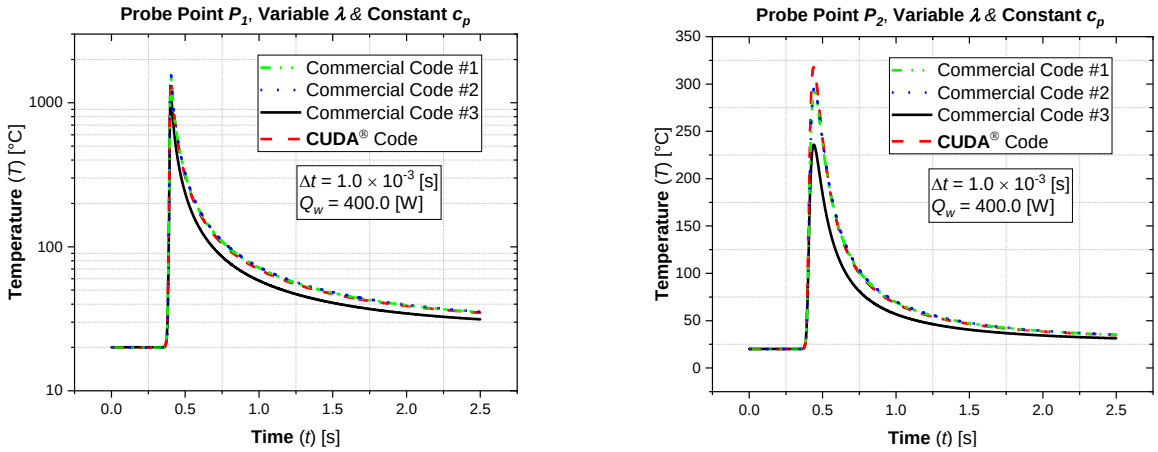

a) b)

Figure 5. Temperature (T) [°C] as a function of time (t) [s] for 400 [W] laser power (Q_w), 1.0 × 10^{-3} [s] time-step size (Δt), variable λ, constant c_p and: a) Probe point $\boldsymbol{P_1}$, b) Probe point $\boldsymbol{P_2}$.

Table 7. Average error (E_{avg}) [%] between CUDA® code and each commercial solution.

Solution	P_1 - Average Error (E_{avg}) [%]	P_2 - Average Error (E_{avg}) [%]
Commercial Code #1	1.751	1.515
Commercial Code #2	2.789	2.396
Commercial Code #3	12.530	**12.572**

The analysis was continued by running the simulations with temperature dependent specific heat (c_p) and constant thermal conductivity (λ). The temperature fields for all solutions are illustrated in Figure 6. The maximum average absolute error reached was 2.323 % between CUDA® code and commercial code #1 for probe point P_1. The average error values are tabulated in Table 8.

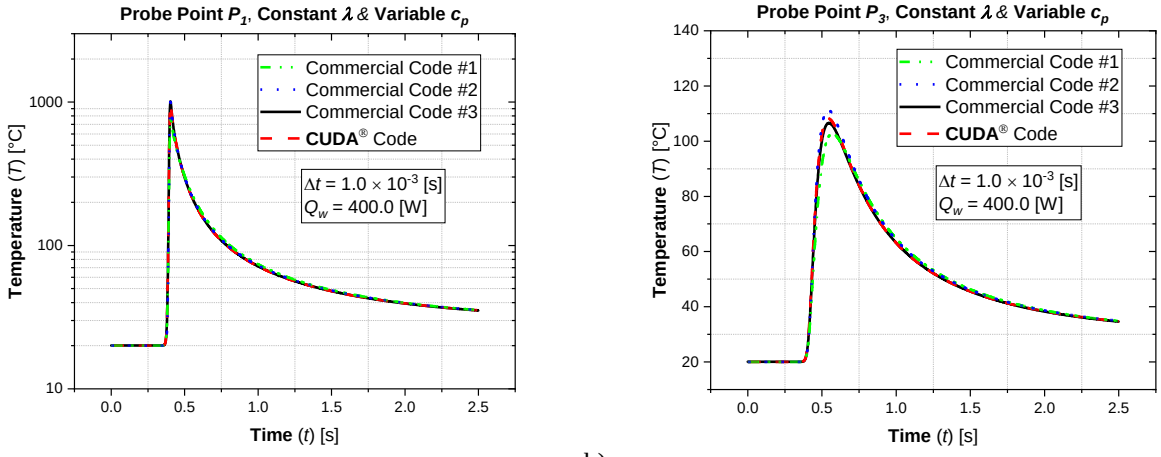

a) b)

Figure 6. Temperature (T) [°C] as a function of time (t) [s] for 400 [W] laser power (Q_w), 1.0 × 10^{-3} [s] time-step size (Δt), constant λ, variable c_p and: a) Probe point $\boldsymbol{P_1}$, b) Probe point $\boldsymbol{P_3}$.

Table 8. Average absolute error (E_{avg}) [%] between CUDA® code and each commercial solution.

Solution	P_1 - Average Error (E_{avg}) [%]	P_3 - Average Error (E_{avg}) [%]
Commercial Code #1	**2.323**	1.840
Commercial Code #2	1.048	1.166
Commercial Code #3	0.262	0.360

Finally, the pure heat conduction investigation was finished by running the simulations with both the specific heat (c_p) and thermal conductivity (λ) set as temperature dependent properties. The maximum average absolute error achieved was 4.727 % between CUDA® code and commercial code #1, for probe point P_3. The average error values are tabulated in Table 9.

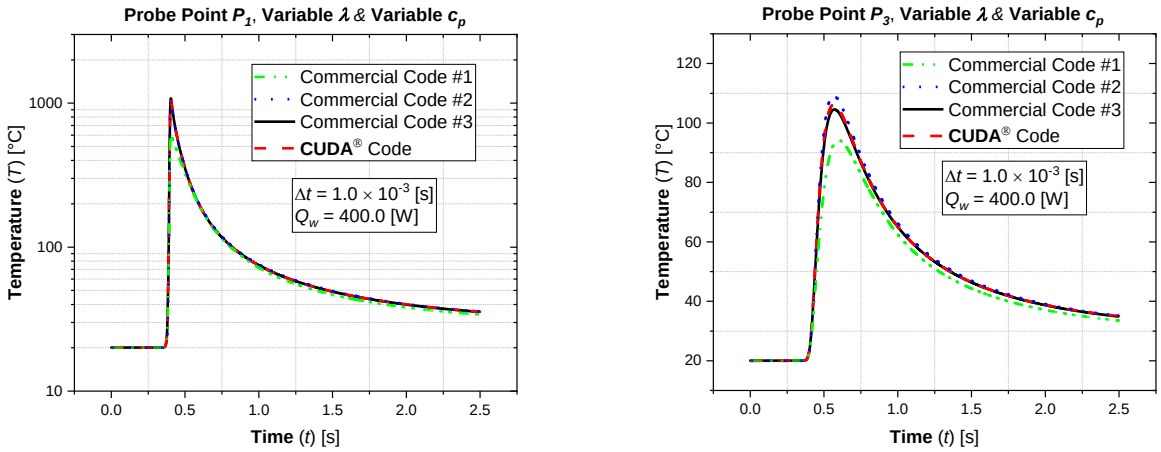

a) b)

Figure 7. Temperature (T) [°C] as a function of time (t) [s] for 400 [W] laser power (Q_w), 1.0 × 10^{-3} [s] time-step size (Δt), variable λ, variable c_p and: a) Probe point $\boldsymbol{P_1}$, b) Probe point $\boldsymbol{P_3}$.

Table 9. Average absolute error (E_{avg}) [%] between CUDA® code and each commercial solution.

Solution	P_1 - Average Error (E_{avg}) [%]	P_3 - Average Error (E_{avg}) [%]
Commercial Code #1	4.330	**4.727**
Commercial Code #2	0.969	1.099
Commercial Code #3	0.271	0.473

3.2 Heat Conduction with Phase Change

The code verification analysis was continued by elevating the laser heat source power (Q_w) to 1200.0 [W], thus resulting in temperature values greater than the melting point of the SAE 1020 steel specimen (T_m = 1450.0 °C). Here, the investigation was aimed at comparing the effects of the phase change modeling on the temperature profiles provided by all codes. Hence, the resulting temperature for all solutions are presented in Figure 8. The maximum average absolute error achieved was 4.543 % between CUDA® code and commercial code #2 for probe point P_2. The average error values are shown in Table 10.

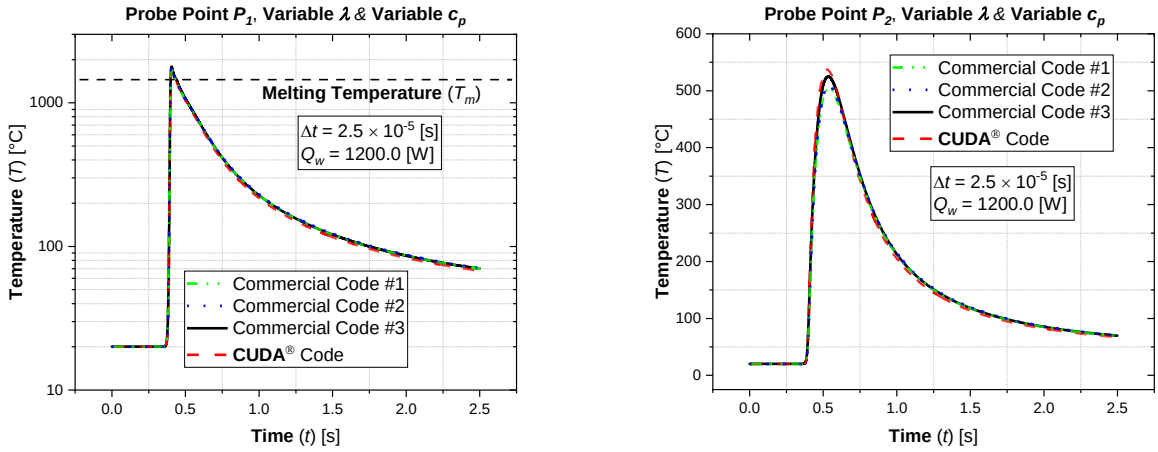

a) b)

Figure 8. Temperature (T) [°C] as a function of time (t) [s] for 1200 [W] laser power (Q_w), 2.5 × 10^{-5} [s] time-step size (Δt), variable λ, variable c_p and: a) Probe point ***P1***, b) Probe point ***P2***.

Table 10. Average absolute error (E_{avg}) [%] between CUDA® code and each commercial solution.

Solution	P_1 - Average Error (E_{avg}) [%]	P_2 - Average Error (E_{avg}) [%]
Commercial Code #1	3.291	3.076
Commercial Code #2	3.178	**4.543**
Commercial Code #3	3.559	2.857

3.3 Computational Performance

Lastly, the investigation was finished by comparing the computational performance achieved by each computational methodology. All commercial code solutions were run with six CPU processing nodes parallelization (n_p = 6). For the commercial solutions investigated here, a higher number of processing nodes results in either no significative processing time reduction or a slightly increase in it. Finally, the processing time and speedup performance comparison for the case with 1200 [W] laser power (Q_w), 2.5 × 10^{-5} [s] time-step size (Δt), variable λ, variable c_p is presented in Figure 9. The required simulation time for the CUDA® code solution running on a RTX 4090 graphics card was also added to enrich the analysis.

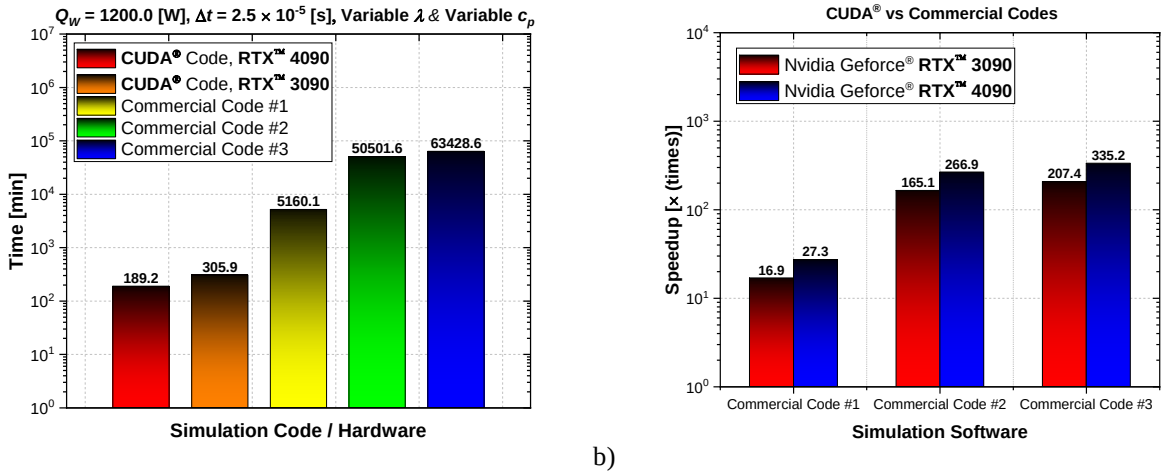

a) b)

Figure 9. Processing comparison for 1200 [W] laser power (Q_w), 2.5 × 10^{-5} [s] time-step size (Δt), variable λ, variable c_p: a) Total time [s] versus applied code / hardware, b) Total speed up reached [× (times)] versus commercial codes.

4. CONCLUSION

The following conclusions were achieved through the development of the present research:

- The CUDA® code solution presented good matching with top-rated commercial codes that have already been submitted to decades of intensive debugging processes;
- In opposition to the belief of many researchers, the investigation has proven the great processing capabilities of GPUs in performing double precision accuracy calculations;

- The GPU chip architecture has proven to be better suited for parallelization than recent modern CPU layouts. This design characteristic resulted speedups ranging from 16.9 to 335.2 times faster than a CPU;
- The Thermal Design Power (TDP) of a powerful GPU is nearly three times higher than that of a high-end CPU. However, much electricity power is still saved since the task is performed hundreds of times faster.

5. ACKNOWLEDGEMENTS

The authors would like to thank CAPES (an agency of the ministry of education of Brazil), CNPq (an agency of the ministry of Science, Technology, Innovations, and Communications of Brazil) and PETROBRAS (a Brazilian multinational company) for the invaluable financial support.

6. REFERENCES

Aboul Khail, A., & Erien, A. (2023). A Review: CFD Approaches of Plate Heat Exchangers. *Archives of Computational Methods in Engineering*, 1157 - 1165.

Benzi, M. (2009). *Key Moments in the History of Numerical Analysis.* Emory University, Atlanta, GA: Department of Mathematics and Computer Science.

Cheung, Y., & Zinkiewicz, O. (1965). Plates and tanks on elastic foundations - an application of finite element method. *International Journal of Solids and Structures*, 451 - 461.

Clough, R., & Felippa, C. (1968). A Refined Quadrilateral Element for Analysis of Plate Bending. *Proceedings of the 2nd Conference on Matrix Methods in Structural Mechanics*.

Courant, R. (1943). Variational Methods for the Solution of Problems of Equilibrium and Vibrations. *Bulletin of the American Mathematical Society*, 1 - 23.

Courant, R., Friedrichs, K., & Lewy, H. (1928). On the Partial Difference Equations of Mathematical Physics. *Matematische Annalen*, 32 - 74.

Crank, J. (1984). *Free and Moving Boundary Problems.* Oxford, UK: Oxford University Press.

Curtiss, J. (1953). Methods for the Iteration of Linear Operators. *Journal of Mathematics and Physics*.

de Azevedo, A., Magalhães, E., da Silva, R., & Lima e Silva, S. (2022). A comparison between nonlinear and constant thermal properties approaches to estimate the temperature in LASER welding simulation. *Case Studies in Thermal Engineering*, 102135.

Ikushima, K., & Shibahara, M. (2014). Prediction of residual stresses in multi-pass welded joint using Idealized Explicit FEM accelerated by a GPU. *Computational Materials Science*, 62 - 67.

Irons, B., & Barlow, J. (1964). Comment on "Matrices for the direct stiffness method". *AIAA Journal*, 403 - 404.

Ju, P., Li, M., & Wang, J. (2022). Review of Research Advances in CFD Techniques for the Simulation of Urban Wind Environments. *Fluid Dynamics & Materials Processing*, 449 - 462.

Ma, N. (2016). An accelerated explicit method with GPU parallel computing for thermal stress and welding deformation of large structure models. *International Journal of Advanced Manufacturing Technology*, 2195 - 2211.

Magalhães, E., dos Santos Paes, L., Pereira, M., da Silveira, C., de Souza Pinto Pereira, A., & Lima e Silva, S. (2018). A thermal analysis in laser welding using inverse problems. *International Communications in Heat and Mass Transfer*, 112 - 119.

Montazeri, H., & Blocken, B. (2013). CFD simulation of wind-induced pressure coefficients on buildings with and without balconies: Validation and sensitivity analysis. *Building and Environment*, 137 - 149.

Nascimento, E., Magalhães, E., & dos Santos Paes, L. (2023). A literature review in heat source thermal modeling applied to welding and similar processes. *The International Journal of Advanced Manufacturing Technology*, 2917 - 2957.

Patankar, S. V. (1980). *Numerical Heat Transfer and Fluid Flow.* Boca Raton: CRC Press.

Philips, H. B., & Wiener, N. (1923). Nets and the Dirichlet Problem. *Journal of Mathematics and Physics*.

Richardson, L. (1910). The Approximate Arithmetical Solution by Finite Differences of Physical Problems Involving Differential Equations, with an Application to the Stresses in a Masonry Dam Trans. *Proceedings of the Royal Society of London*, 307 - 357.

Whittaker, E., & Robinson, G. (1924). *The Calculus of Observations; a Treatise on Numerical Mathematics.* London: Blackie and Son Limited.

Zhang, X., Guo, X., Weng, Y., Zhang, X., Lu, Y., & Zhao, Z. (2023). Hybrid MPI and CUDA paralleled finite volume unstructured CFD simulations on a multi-GPU system. *Future Generation Computer Systems*, 1 - 16.

7. RESPONSIBILITY NOTICE

The authors are the only responsible for the printed material included in this paper.